ISSN 1063-7834, Physics of the Solid State, 2021, Vol. 63, No. 12, pp. 1785–1794. © Pleiades Publishing, Ltd., 2021.
ISSN 1063-7834, Physics of the Solid State, 2021. © Pleiades Publishing, Ltd., 2021.
Russian Text © The Author(s), 2021, published in Fizika Tverdogo Tela, 2021, Vol. 63, No. 10, pp. 1462–1470.

Mechanisms of the Magnetoresistance Hysteresis in a Granular HTS with the Paramagnetic Contribution by the Example of $HoBa_2Cu_3O_{7-\delta}$

S. V. Semenov[a, b], D. M. Gokhfel'd[a, b], K. Yu. Terent'ev[a], and D. A. Balaev[a, b, *]

[a] *Kirensky Institute of Physics, Krasnoyarsk Scientific Center, Siberian Branch, Russian Academy of Sciences, Krasnoyarsk, 660036 Russia*

[b] *Siberian Federal University, Krasnoyarsk, 660041 Russia*

**e-mail: dabalaev@iph.krasn.ru*

Received May 14, 2021; revised May 14, 2021; accepted May 25, 2021

Abstract—The hysteretic behavior of magnetoresistance $R(H)$ of the granular high-temperature superconductor (HTS) $HoBa_2Cu_3O_{7-\delta}$ has been investigated. The YBCO superconductors with a rare-earth element (Nd, Ho, Er, Sm, Yb, or Dy) with the magnetic moment in the yttrium site are characterized by a significant paramagnetic contribution to the total magnetization. The main goal of this study has been to establish the possible effect of this paramagnetic contribution on the magnetotransport properties, which are determined by tunneling of superconducting current carriers through the grain boundaries. An analysis of the results obtained basing on the concept of an effective field in the intergrain medium showed that the distribution of the magnetic induction lines from the paramagnetic moments is fundamentally different from that of the Meissner currents and Abrikosov vortices. The magnetic induction lines from the paramagnetic moments are not concentrated in the region of grain boundaries and therefore insignificantly affect the magnetotransport properties of a granular HTS. At the same time, the magnetic induction lines are strongly concentrated in the grain boundaries, which is caused by the Meissner currents and Abrikosov vortices, due to the features of their properties. Specifically, the magnetic flux compression determines the magnetotransport (in particular, the $R(H)$ hysteresis) properties of granular HTSs, including 1–2–3 ones, with a rare-earth ion with the magnetic moment.

Keywords: $HoBa_2Cu_3O_{7-\delta}$ granular HTS, paramagnetic contribution, magnetoresistance hysteresis, effective field, grain boundaries

DOI: 10.1134/S1063783421100334

1. INTRODUCTION

The magnetotransport properties of granular high-temperature superconductors (HTSs) are explained by the well-known fact of implementation of a two-level superconducting system in these objects [1–3]. The levels are HTS grains, which represent a strongly superconducting subsystem, and grain boundaries, in which the superconducting properties are essentially suppressed and the superconducting current is transmitted through them by means of the Josephson effect. A fairly large number of studies on granular HTSs have been devoted to the mechanisms of dissipation in the grain boundary subsystem in an external magnetic field [4–15]. However, in these studies, the grain boundary subsystem where the dissipation occurs has often been considered independent, disregarding the irreversible character of the field dependences of magnetoresistance $R(H)$ [16–25] and critical current $I_C(H)$ [26–29], as well as the temperature dependences of magnetoresistance $R(T)$ [30–35] measured in an external magnetic field. The explanation of the nontrivial behavior of the magnetotransport characteristics has already required the interaction between the subsystems of grains and grain boundaries to be taken into account.

At different times, different models of penetration of a magnetic field into the intergrain medium [36] and HTS grains [18–21, 37–40] were proposed and the redistribution of the magnetic induction lines in the intergrain medium was considered [41]. It is logical that the external field first penetrates into the subsystem of grain boundaries. The value of such a penetration field is rather small; for example, for the yttrium system, these are fractions of oersted at the nitrogen temperature and several oersted at lower temperatures. The penetration of the magnetic flux into grains occurs already in strong external fields: tens of oersted at the nitrogen temperature and hundreds of oersted at lower temperatures. However, the especially interesting feature turned out to be the effect of the

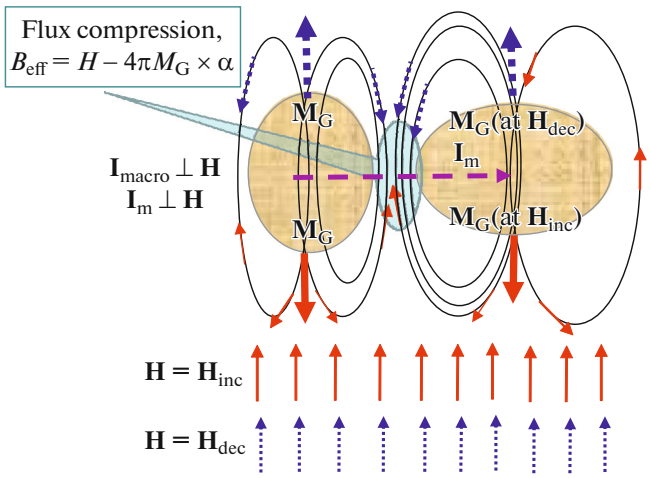

Fig. 1. Schematic of the distribution of the magnetic induction lines from magnetic moments $\mathbf{M}_G$ of HTS grains. Grains are ovals, the space between them is the intergrain boundary, $\mathbf{I}_m$ is the microscopic current (tunneling from the left grain to the right one), and $\mathbf{I}_{macro}$ is the macroscopic current through the sample ($\mathbf{I}_{macro} \perp \mathbf{H}$). The directions of $\mathbf{M}_G$ and magnetic induction lines relative to the external field are shown by solid ($\mathbf{H} = \mathbf{H}_{inc}$, the field increases) and dashed ($\mathbf{H} = \mathbf{H}_{dec}$, the field decreases) arrows.

magnetic moments of HTS grains on the resulting field in the grain boundaries.

Let us consider this effect in more detail. The magnetization of a superconductor is determined by the Meissner currents, which are responsible for the diamagnetic behavior, and the trapped flux (the Abrikosov vortices). The superposition of these contributions yields a typical magnetic hysteresis loop, for which magnetization M takes negative values in the increasing external field ($H = H_{inc}$, $H_{inc} > 0$) and positive values in the decreasing external field ($H = H_{dec}$, $H_{dec} > 0$). Consequently, magnetic moments $\mathbf{M}_G$ of grains are directed antiparallel to the external field at $H = H_{inc}$ and parallel $\mathbf{H}$ to it at $H = H_{dec}$. In the case of a granular HTS, we can arrive at a picture of redistribution of the magnetic induction lines in the grain boundaries for two adjacent HTS grains (see a schematic in Fig. 1). The superconducting current carriers (in Fig. 1, this is microscopic current $\mathbf{I}_m$) tunnel through the grain boundary; the tunneling occurs in the total field, which is a superposition of external field $\mathbf{H}$ and the field induced by magnetic moments $\mathbf{M}_G$. The analysis of the mutual direction of $\mathbf{H}$ and magnetic induction lines in the grain boundary (Fig. 1) shows that, at $\mathbf{I}_m \perp \mathbf{H}$, the total (effective) field $B_{eff}(\mathbf{I}_m \perp B_{eff})$ is expressed as [29, 42]

$$B_{eff} = H - 4\pi M_G \alpha. \quad (1)$$

Coefficient α includes the average demagnetizing factor of these grains and reflects the crowding of the force lines in the intergrain space due to the flux compression. The possible compression of the magnetic flux was first noted in [41]. If we average the parameter α, already over all the grain boundaries, where $\mathbf{I}_m \perp \mathbf{H}$, and will operate with the magnetization of a material ($M(H) = \Sigma M_G(H)$), then we obtain an expression similar to (1) for the effective field B_{eff} in the intergrain medium. For the dissipation processes, the B_{eff} sign (or the $\mathbf{B}_{eff}$ direction relative to $\mathbf{H}$) is no longer important; as a result, Eq. (1) is rewritten as

$$B_{eff}(H) = |H - 4\pi M(H) \times \alpha|. \quad (2)$$

This equation can be used to reproduce the shape of the magnetoresistance hysteresis $R(H)$ using the experimental data on the magnetization and taking $R(H) \sim B_{eff}(H)$ [42–44]. In addition, Eq. (2) describes the shape of the $I_C(H)$ hysteresis, if we assume $I_C \sim 1/R$. A detailed comparison of the experimental $R(H)$ dependences with the $B_{eff}(H)$ dependences showed that the parameter α (Eq. (2)) is rather large: $\alpha \approx 20$–25 at the orientation $\mathbf{H} \perp \mathbf{I}_{macro}$ ($\mathbf{I}_{macro}$ is the macroscopic current direction) and $\alpha \approx 12$–14 at the orientation $\mathbf{H} \parallel \mathbf{I}_{macro}$ [35, 42–45]. This allowed us to speak about the strong effect of the magnetic flux compression in the intergrain medium (see Fig. 1). It was found that, for the yttrium HTS system, the parameter α is almost temperature-independent (from the temperatures close to the critical one to 4.2 K) [46–49] and does not strongly vary in the samples with different current-carrying capacities (critical current densities) [50]. The use of effective field B_{eff} instead of external field H in the well-known equation $R = f(H)$ (f is the Arrhenius-type function) made it possible to quantitatively describe the experimental $R(H)$ hysteretic dependences, as well as the $R(T)$ dependences (at H = const) [51]. Thus, the above-described concept of the effective field in the intergrain medium, with allowance for the flux compression, explains well the observed dissipation behavior in external fields.

Equation (2) operates with a macroscopic characteristic: specific magnetization $M(H)$ of a granular HTS material. An interesting question arising here is how the additional magnetic subsystem in HTS grains will affect transport of superconducting current carriers through the grain boundaries. Objects for these studies can be 1–2–3 granular HTSs with the complete or partial substitution of magnetic ions for a rare-earth element (classical yttrium). In the $Re_1Ba_2Cu_3O_{7-\delta}$ (Re is the rare-earth element) HTS systems, the magnetic moment of Re (Nd, Ho, Er, Sm, Yb, or Dy) almost does not affect superconducting transition temperature T_C. However, the shape of the magnetic hysteresis loops $M(H)$ significantly changes if Re has the magnetic moment [52–56]. Although the magnetic ordering of the Re subsystem occurs at temperatures of no higher than 3 K [57], above this temperature, the Re subsystem makes a significant paramagnetic contribution to the total mag-

netization of the HTS sample. In this case, as was noted in [52, 56], the contributions of the superconducting and Re subsystems can be considered almost independent. In this study, we examined the magnetoresistance of the $HoBa_2Cu_3O_{7-\delta}$ granular HTS in order to establish how the paramagnetic subsystem affects the effective field in the intergrain medium.

2. EXPERIMENTAL

The investigated $HoBa_2Cu_3O_{7-\delta}$ HTS sample was prepared by the solid-state synthesis from the corresponding oxides with three intermediate grindings. According to the scanning electron microscopy data obtained on a Hitachi-TM 4000 electron microscope, the average grain size was 3–4 μm.

The magnetotransport measurements were performed by a four-probe method. A sample 0.14 × 0.2 × 7 mm^3 in size was prepared from the synthesized tablet; transport current I was directed along the major axis of the sample. The external field was set by an electromagnet during the $R(T)$ measurements above 77 K and by a superconducting solenoid during the $R(H)$ measurements at $T = 4.2$ K. In both cases, the external field was perpendicular to the macroscopic transport current ($\mathbf{H} \perp \mathbf{I}_{macro}$). The $R(H)$ dependences at a temperature of 4.2 K were measured by placing the sample directly in liquid helium. This allowed us to avoid sample heating by the heat released at the contacts during the flow of a current of ~100–200 mA.

The magnetic properties (the $M(H)$ and $M(T)$ dependences) were measured with a vibrating sample magnetometer [58] under the external conditions (including the external field variation rate) similar to those of the $R(H)$ measurements. A part of the magnetic measurements was performed on a LakeShore VSM 8604 system. Before the measurements, the sample was cooled in zero external field.

3. RESULTS AND DISCUSSION

3.1. Superconducting and Magnetic Properties of $HoBa_2Cu_3O_{7-\delta}$

Figure 2 shows the $R(T)$ dependences for the investigated sample obtained in fields of 10, 100, and 1000 Oe. The onset of the superconducting transition (a sharp decrease in the resistance) occurs at a temperature of ~92.5 K, which coincides with the data of the magnetic measurements (at $H = 10$ Oe) shown in the inset in Fig. 2. The two-step shape of the $R(T)$ dependences in Fig. 2 and the strong effect of the relatively weak fields on the broadening of the smooth part of the resistive transition are typical of granular HTSs [1, 5, 6, 12, 29, 30, 35, 47–51, 59–63]. Such a behavior of the $R(T)$ dependences reflects the presence of two superconducting subsystems, as noted in Introduction. Obviously, the smooth part of the resistive transition corresponds to dissipation in the subsystem of grain boundaries.

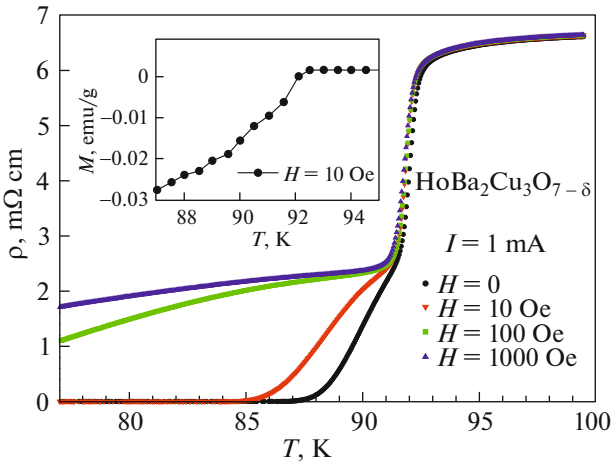

Fig. 2. $R(T)$ dependences for $HoBa_2Cu_3O_{7-\delta}$ in different external fields. Inset: temperature dependence of magnetization in a field of $H = 10$ Oe in the vicinity of T_C.

Figure 3 shows the temperature dependence of the magnetization (in M^{-1} vs T coordinates) measured in a field of $H = 10$ kOe in the temperature range above 100 K. It can be seen that the $M(T)$ dependence of the investigated $HoBa_2Cu_3O_{7-\delta}$ sample exhibits the paramagnetic behavior: the experimental data hit the linear dependence $M^{-1} \sim T$ shown by a straight. It can be seen that this linear dependence crosses the T axis in the negative temperature range, which is indicative of the antiferromagnetic ordering of the holmium magnetic moments. The corresponding Curie–Weiss temperature is –13 K. The inset in Fig. 3 shows portions of the magnetic hysteresis loops at the temperatures corresponding to the region of existence of superconductivity. In addition to the superconducting response, there is the pronounced paramagnetic contribution (the visible slope of the $M(H)$ dependences in sufficiently strong fields), which decreases with temperature. The largest contribution from the subsystem of the holmium magnetic moments is observed at $T = 4.2$ K. The results obtained are consistent with the data reported in [52, 54, 56]. Note that the magnetic ordering temperature for $HoBa_2Cu_3O_{7-\delta}$ is 0.19 K [64].

Since below we analyze the magnetoresistance at a temperature of 4.2 K, where the paramagnetic (hereinafter, PM) contribution is the largest, let us focus on the behavior of the magnetization hysteresis loop $M(H)$ at $T = 4.2$ K (Fig. 4). In contrast to the classical hysteresis loop of a type-II superconductor, the $M(H)$ dependence shown in this figure (hereinafter, $M_{tot}(H)$ contains the PM contribution. Due to the presence of the PM contribution, the magnetization becomes positive with an increase in the external field already in

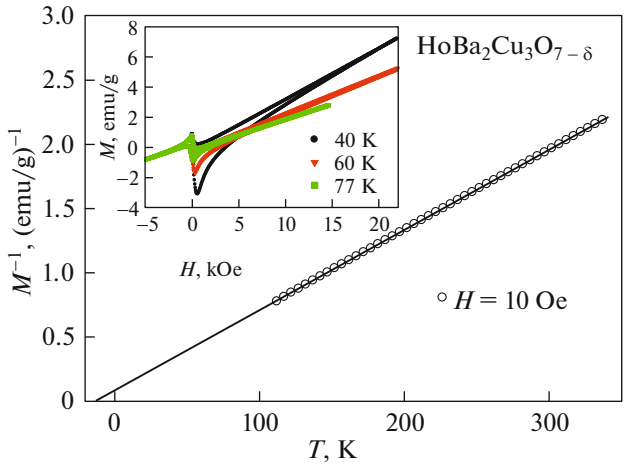

Fig. 3. Temperature dependence of reverse magnetization $M^{-1}(T)$ for $HoBa_2Cu_3O_{7-\delta}$ in a field of $H = 10$ kOe in the temperature range above T_C (symbols). A straight solid line indicates the fulfillment of the Curie–Weiss law (see Subsection 3.1). Inset: sections of the magnetic hysteresis loops at the indicated temperatures ($T < T_C$).

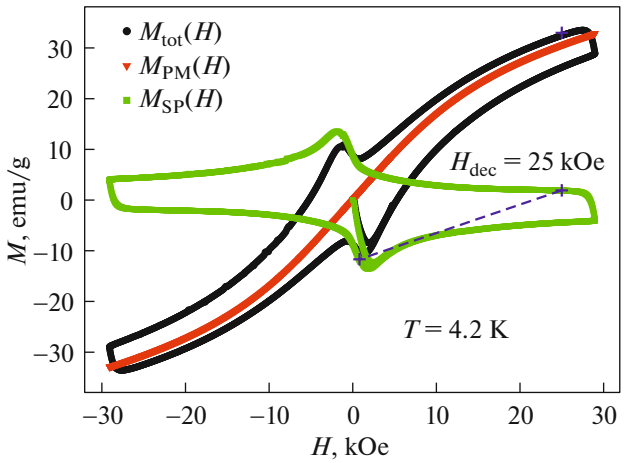

Fig. 4. Magnetic hysteresis loop $M_{tot}(H)$ for the $HoBa_2Cu_3O_{7-\delta}$ sample at $T = 4.2$ K and separated paramagnetic $M_{PM}(H)$ (see Subsection 3.1) and superconducting $M_{SP}(H)$ contributions (see Subsection 3.1). The plus marks connected by a dashed straight in the $M_{SP}(H)$ dependence are the magnetization values (at H_{dec} = 25 kOe and H_{inc} = 1.1 kOe) corresponding to the condition $R(H_{dec} = 25\ \text{kOe}) = \text{const}$ for the $R(H)$ dependence in Fig. 5a (see Subsection 3.2).

relatively weak fields. To obtain an unperturbed superconducting (hereinafter, SP) magnetization hysteresis loop, the theoretical dependence of magnetization $M_{PM}(H) = NgJ\mu_B B_J(gJ\mu_B H/kT)$ for a paramagnet, where N is the number of magnetic ions per unit volume, μ_B is the Bohr magneton, k is the Boltzmann constant, g is the Lande factor, J angular momentum quantum number, and B_J is the Brillouin function, was subtracted from the experimental $M_{tot}(H)$ dependence. When separating the PM and SP contributions, the values for Ho ($J = 8$, $g = 1.25$) were used and the magnetic ion concentration N served as a fitting parameter. The criterion for adequacy of the separation of the SP and PM contributions was the absence of a slope of the SP hysteresis loop in strong fields. The result of extracting of the PM and SP contributions is shown in Fig. 4. The PM contribution corresponds to a Ho concentration of 2.32×10^{21} cm^{-3} in $HoBa_2Cu_3O_{7-\delta}$ in low fields and 3.01×10^{21} cm^{-3} at $H = 30$ kOe. These values are smaller than a theoretical value of 5.79×10^{21} cm^{-3} and the similar behavior was observed in the analysis of the $ReBa_2Cu_3O_{7-\delta}$ systems [52, 54, 56]. This is apparently due to the partial screening of Ho ions inside the superconductor from the external magnetic field. The PM contribution is most likely made by only Ho ions located in the normal cores of the Abrikosov vortices and in the surface region of grains with a thickness comparable with the magnetic field penetration depth [54, 56]. The hysteresis loop built after the separation of the SP contributions (Fig. 4) has a shape typical of granular HTSs.

To determine the critical current density from the hysteresis loop, we used the relation following from the critical state model [65]: J_C (A cm^{-2}) = $30\Delta M$ (emu cm^{-3})/d (cm), where $\Delta M = M(H_{dec}) - M(H_{inc})$ is the difference between the decreasing and increasing hysteresis branches and d is the characteristic size of the current circulation. For a granular HTS, the d value should coincide with the average grain size. Along with the scanning electron microscopy, the d value can be estimated from the asymmetry of the superconducting hysteresis loop. According to the results reported in [66], $d \approx 2\lambda/[1 - (\Delta M/|2M(H_{inc})|)^{1/3}]$, where λ is the London penetration depth ($\lambda \approx 150$ nm for the Y–Ba—Cu–O system [67]). Our estimates are $d \approx 3 \times 10^{-4}$ cm and $J_C = 6.8 \times 10^6$ A cm^{-2}. The d value corresponds to the average grain size in the sample (see Section 2); therefore, the obtained J_C value is the maximum density of the intragrain current.

3.2. Analysis of the R(H) Hysteresis. Contributions of the Meissner Currents, Abrikosov Vortices, and Paramagnetic Subsystem to the Effective Field in the Intergrain Medium

The $R(H)$ dependences at $T = 4.2$ K for the investigated $HoBa_2Cu_3O_{7-\delta}$ sample are shown in Fig. 5. The presented data correspond to transport currents of $I = 180$ mA (Fig. 5a) and 100 mA (Fig. 5b) obtained upon cycling the external field to maximum values of $H_{max} = \pm 30$ kOe (Fig. 5a) and $H_{max} = \pm 10$ kOe (Fig. 5b). Arrows in the figure correspond to the direc-

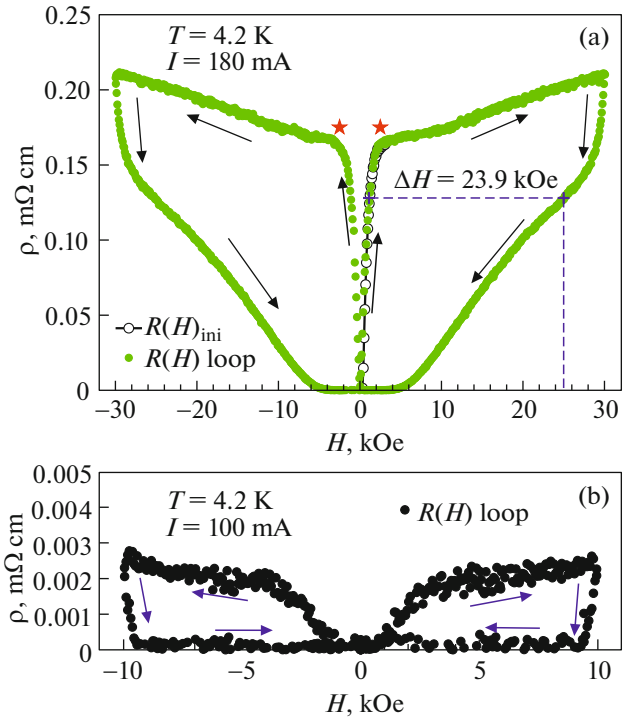

Fig. 5. Magnetoresistance $R(H)$ of the $HoBa_2Cu_3O_{7-\delta}$ sample at $T = 4.2$ K and the indicated values of transport current I. The $R(H)$ loop dependences correspond to multiple cycling of the field up to the maximum value H_{max} ((a) ±30 and (b) ±10 kOe), and $R(H)_{ini}$ is the initial dependence of the magnetoresistance. Arrows correspond to the direction of the external field variation. The horizontal dashed line in (a) shows the field width of the $R(H)$ hysteresis at $H_{dec} = 25$ kOe.

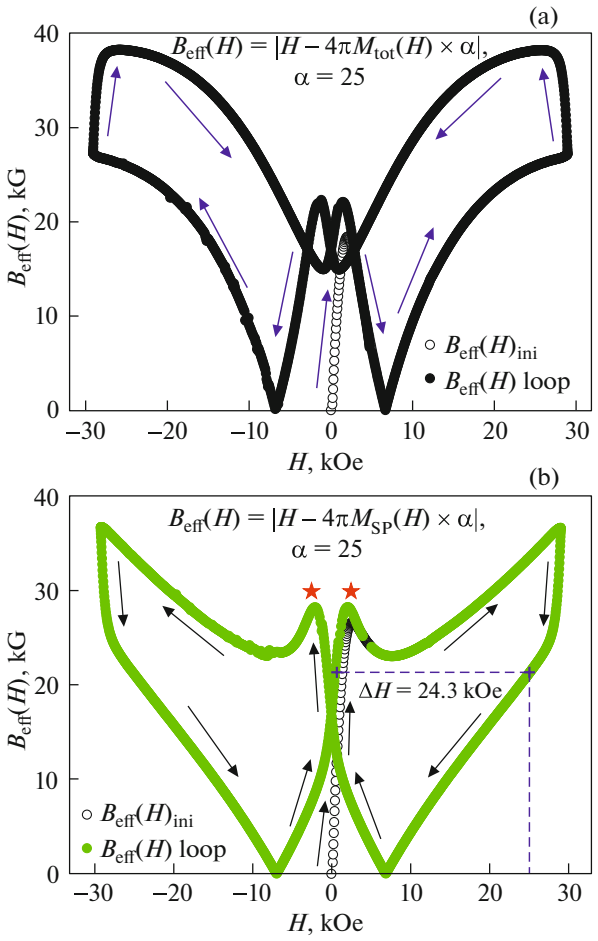

Fig. 6. Hysteretic dependence $B_{eff}(H)$ of the effective field in the intergrain medium on external field H plotted using Eq. (2) from the data in Fig. 3 at $\alpha = 25$ for (a) $M(H) = M_{tot}(H)$ and (b) $M(H) = M_{SP}(H)$. The $B_{eff}(H)$ loop dependence corresponds to the cycling of the external field up to $H_{max} = \pm 30$ kOe and the $B_{eff}(H)_{ini}$ dependence is the initial course. Arrows show the direction of the external field variation. Note the different directions of the hysteresis in (a) and (b). The horizontal dashed line shows the field width of the $B_{eff}(H)$ hysteresis at $H_{dec} = 25$ kOe.

tion of the external field variation; for the data from Fig. 5a, the initial $R(H)_{ini}$ dependence is shown. First of all, note that the shape of the $R(H)$ hysteretic dependence and the relative positioning of the magnetoresistance branches $R(H_{inc})$ (the field increases) and $R(H_{dec})$ (the field decreases) are similar to those observed by us previously for $YBa_2Cu_3O_{7-\delta}$ [47–50].

Let us analyze the obtained $R(H)$ dependences using the concept of the effective field B_{eff} in the intergrain medium described in Introduction. In different theoretical concepts, the magnetoresistance of a type-II superconductor is a monotonic increasing function of the external field [4–12, 51, 68]. For the intergrain medium, the magnetoresistance is a function of B_{eff}, which depends on the external field. Hence, the $B_{eff}(H)$ dependence should behave similarly to the $R(H)$ dependence. Figure 6a shows the $B_{eff}(H)$ dependence built from the experimental $M_{tot}(H)$ dependence for $HoBa_2Cu_3O_{7-\delta}$ (Fig. 4) using Eq. (2). Here, based on the results of previous studies [45–51] for $YBa_2Cu_3O_{7-\delta}$, the parameter α was also taken to be 25. The comparison of the $R(H)$ data (Fig. 5a) and the $B_{eff}(H)$ data showed no agreement (Fig. 6a). The most important difference is that the $R(H)$ hysteresis goes clockwise (for the positive H values) and the $B_{eff}(H)$ hysteresis, counterclockwise. Note that a decrease in the parameter α does not lead to agreement between the $R(H)$ and $B_{eff}(H)$ dependences: the $B_{eff}(H)$ hysteresis becomes narrow.

The magnetic hysteresis loop of a type-II superconductor arises due to the circulation of the Meissner currents and the penetration and pinning of the Abrikosov vortices. The contributions of the Meissner currents and Abrikosov vortices have different signs with respect to the external field. The effect of the Abrikosov vortices and Meissner currents on the effective field of grain boundaries will also be different. To

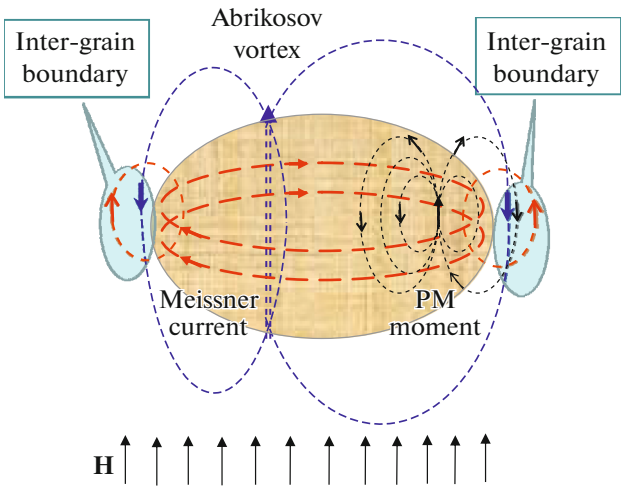

Fig. 7. Schematic of directions of the magnetic induction lines from the Abrikosov vortices, Meissner currents, and PM moments inside and outside (grain boundaries) a grain in a granular HTS. The case $H > 0$ is illustrated.

illustrate the aforesaid, Fig. 7 schematically shows the magnetic induction lines from the Abrikosov vortices and Meissner currents. Note that the pure effect of the Abrikosov vortices on B_{eff} and ultimately on the dissipation manifests itself in the nonzero resistance at $H = 0$ after applying an external field [29, 35, 42–49], as well as in the relaxation of the residual resistance with time (the latter is related to the magnetization relaxation caused by the escape of the vortices from the superconductor) [42, 69]. In the presence of a paramagnetic contribution in HTS grains, which is also schematically shown in Fig. 7 (in the form of one spin), the magnetic induction lines from the PM moments should close, in particular, across the grain boundary. Therefore, the contribution of the PM moments to the effective field B_{eff} should have the same sign as that of the Abrikosov vortices. Quantitatively, the contribution of M_{PM} to the total magnetization $M_{tot}(H)$ of the $HoBa_2Cu_3O_{7-\delta}$ sample in strong fields is quite large (see Fig. 4); it exceeds the contribution of the superconducting subsystem. Therefore, when $M_{tot}(H)$ is substituted into Eq. (2), the expected contributions of the Abrikosov vortices and the PM subsystem prevail over the external field and diamagnetism of the Meissner currents. As a result, the $B_{eff}(H)$ dependence is strongly nonmonotonic (Fig. 6a), while the $B_{eff}(H)$ hysteresis goes counterclockwise, which is not observed in the experiment (Fig. 5).

It is logical to analyze the $R(H)$ hysteresis and plot the $B_{eff}(H)$ dependence without the contribution of the PM subsystem. According to Fig. 4, we have $M_{tot}(H) = M_{SP}(H) + M_{PM}(H)$. Then, if only the contribution $M(H) = M_{SP}(H)$ of the superconducting loop is substituted into Eq. (2) instead of $M(H) = M_{tot}(H)$, the obtained $B_{eff}(H)$ dependence at $\alpha = 25$ has a form shown in Fig. 6b. In this case, the behavior of the $B_{eff}(H)$ dependence already describes well the $R(H)$ hysteresis, which is explained as follows. As was shown previously, the $R(H)$ hysteretic dependence has a universal parameter independent of the transport current: the hysteresis field width, which is defined as the segment $\Delta H = H_{dec} - H_{inc}$ under the condition $R(H_{dec}) = R(H_{inc}) = \text{const}$ [29, 46, 48, 69–72]. The length of the horizontal dashed line in Fig. 5a illustrates the value of this parameter at $H_{dec} = 25$ kOe. In this case, $\Delta H = 23.9$ kOe, since the horizontal line in Fig. 5a crosses the magnetoresistance branch $R(H_{inc})$ at $H_{inc} = 1.1$ kOe. The corresponding magnetization M_{SP} in fields of $H_{dec} = 25$ kOe and $H_{inc} = 1.1$ kOe are shown in Fig. 4 (the plus marks connected by a dashed line). The horizontal dashed line in Fig. 6b has the same meaning as in Fig. 5a, but already for the $B_{eff}(H)$ dependence and, at the same value $H_{dec} = 25$ kOe, the ΔH value is 24.3 kOe, which is very close to the data in Fig. 5a. This agreement is only obtained at a sufficiently large parameter $\alpha = 20–25$, which is indicative of the effect of the magnetic flux compression in the intergrain medium (Fig. 1). The flux compression manifests itself in the fact that, for relatively weak fields H_{inc} (several kilooersteds), the B_{eff} value can be tens of kilogauss (see Fig. 6b). In addition, note that the increasing field branches of the $R(H_{inc})$ dependence contain anomalies in the vicinity of $H_{inc} \approx \pm 3$ kOe marked with an asterisk in Fig. 5a. These anomalies correspond to local maxima in the $B_{eff}(H_{inc})$ dependence in Fig. 6b (asterisks) and extrema of the $M_{SP}(H)$ dependence (Fig. 3).

Thus, as an intermediate conclusion, we can state, according to the analysis of the hysteresis of the magnetoresistance of the $HoBa_2Cu_3O_{7-\delta}$ sample basing the concept of an effective field in the intergrain medium, the effect of the PM subsystem (the holmium magnetic moments) almost does not affect the effective field in the intergrain medium and, consequently, the tunneling of superconducting current carriers through the grain boundaries. At the same time, the PM contribution to the total magnetization of the sample is rather large, even in moderate fields (Fig. 4). To explain this, it is worth returning to the schematic representation of the magnetic induction lines in the intergrain medium. Now, instead of one (Fig. 7) or two (Fig. 1) grains, we consider a cross section of the sample with a finite size (Fig. 8) consisting of many grains. The magnetic induction lines from all the contributions (the Meissner currents, Abrikosov vortices, and PM moments) should close not only through the boundaries between neighboring grains, but also through the entire sample, since all the contributions are clearly seen from the magnetic measurement data and only the vortices completely closed inside the sample will not contribute to the total magnetization.

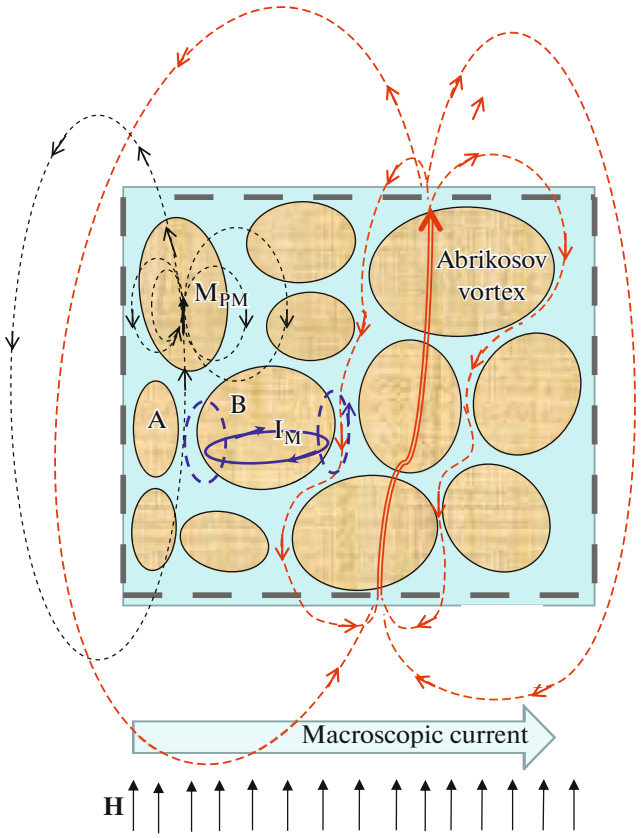

Fig. 8. Schematic of the distribution of magnetic induction lines in a granular HTS of a finite size (the square bounded by dashed lines). Ovals are grains and the space between them is the intergrain medium. The probable trajectories of the magnetic induction lines from the Abrikosov vortices, Meissner currents $\mathbf{I}_M$, and paramagnetic moments $\mathbf{M}_{PM}$ are shown. The directions of the magnetic induction lines correspond to the case $H > 0$.

The Abrikosov vortices can pass through many grains. The vortex field goes beyond a superconducting grain at one point (with a diameter of about two coherence lengths). The magnetic induction lines from the Abrikosov vortex emerging from the upper grain should close in one place: at the beginning of the same vortex on the lowest grain (Fig. 8). The magnetic induction lines from a vortex or a bundle of Abrikosov vortices can be closed both outside the sample and through the intergrain boundaries. It is clear from the general electrodynamics concepts that the highest density of the magnetic induction lines will be around the grain from which the vortex emerges, i.e., in the nearest intergrain gaps. This manifests itself as a flux compression in the intergrain medium, as applied to the subsystem of the Abrikosov vortices.

The Meissner currents ($\mathbf{I}_M$) flow in the planes perpendicular to the external field and the magnetic field from them is equivalent to the field of a closed circular current. The lines of this field must pass through the entire sample, which manifests itself as diamagnetism of the superconducting sample. However, the field induced by the Meissner currents will be maximum near the grain edge, i.e., the grain boundary and, then, in the geometry $\mathbf{H} \perp \mathbf{I}_{macro}$($\mathbf{H} \perp \mathbf{I}_m$) for tunneling, for example, from grain **A** to grain **B** (see Fig. 8), the field from the Meissner current will be parallel to the external field. Then, at the boundary between grains **A** and **B**, we can speak about the strong effect of the field from the Meissner current, which fits into the magnetic flux compression in the intergrain medium and causes a value of the parameter α sufficiently large to describe the $R(H)$ hysteresis.

The magnetic moments of a rare-earth element (holmium) behave like an independent PM subsystem, as evidenced by the results of studies [52, 54, 56] and the results of this study (Figs. 3, 4, Subsection 3.1). The magnetic induction lines from the PM moments can also be closed both through the entire sample and in local regions, both leaving the grain and without leaving it. This is schematically shown in Fig. 8. If these magnetic induction lines are not concentrated in the intergrain spacings, like the magnetic induction lines from the Abrikosov vortices, then the PM contribution should affect the field in the intergrain boundaries much weaker. Hence, the above "negative result," in which the $R(H)$ hysteresis cannot be explained by Eq. (2) using the magnetization $M_{tot}(H)$, indicates that the magnetic induction lines from the PM moments can close, passing through many grains. Then, the concentration in the intergrain medium does not occur.

On the other hand, the spins located near the grain edge should still contribute to the effective field in the intergrain boundary, although without the magnetic flux compression. To take this possibility into account, we rewrite Eq. (2) in the form

$$B_{eff}(H) = \left|H - 4\pi M_{SP}(H) \times \alpha_{SP} - 4\pi M_{PM}(H)\alpha_{PM}\right|. \quad (3)$$

In Eq. (3), $M_{tot}(H) = M_{SP}(H) + M_{PM}(H)$, $\alpha_{SP} = \alpha$, and α_{PM} is the parameter characterizing the possible compression of the magnetic induction lines from the PM moments. Figure 9 presents the $B_{eff}(H)$ dependences calculated using Eq. (3) from the $M_{SP}(H)$ and $M_{PM}(H)$ data shown in Fig. 4 for $\alpha_{SP} = 25$ (as before) and α_{PM} equal to 0, 1, 3, and 5. At $\alpha_{PM} = 0$, the $B_{eff}(H)$ dependence reproduces the data from Fig. 5b and, as shown above, there is good agreement with the hysteresis width ΔH for the $R(H)$ data (see Figs. 6b and 5a). In principle, for the $B_{eff}(H)$ dependence at $\alpha_{PM} = 1$, the parameter ΔH at $H_{dec} = 25$ kOe is 24.8 kOe (the horizontal line $B_{eff}(H) = \text{const}$ intersects with the $B_{eff}(H_{inc})$ dependence at $H_{inc} = 0.2$ kOe), which is also close to the ΔH value of the $R(H)$ dependence (23.9 kOe, see Fig. 5a). With a further increase in α_{PM}, as can be seen in Fig. 9, the horizontal dashed line $B_{eff}(H_{dec} = 25\ \text{kOe}) = \text{const}$ no longer intersects the $B_{eff}(H_{inc})$

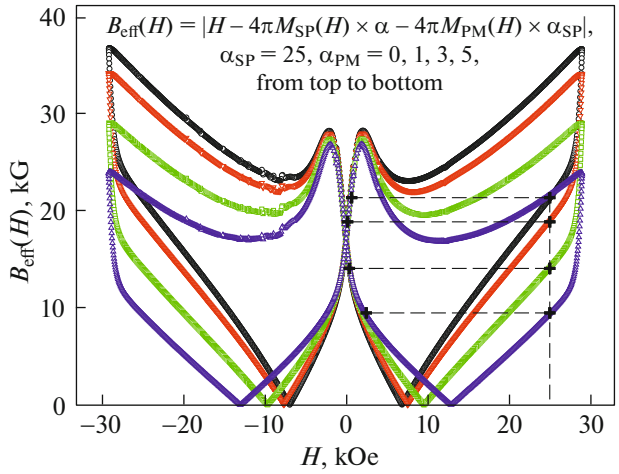

Fig. 9. Dependences of effective field $B_{eff}(H)$ in the intergrain medium on external magnetic field H built according to Eq. (3) using the data from Fig. 3 at different α_{PM}. Horizontal dashed lines illustrate the field width of the $B_{eff}(H)$ hysteresis at $H_{dec} = 25$ kOe.

branch, but crosses the descending field $B_{eff}(H_{dec})$, which is in poor agreement with the behavior of the $R(H)$ dependence (Fig. 5a). Another manifestation of the disagreement with the behavior of the magnetoresistance hysteresis is a fairly strong shift of the $B_{eff}(H_{dec})$ minimum with increasing α_{PM}. The region of the field H_{dec} in the vicinity of this minimum corresponds to zero resistance of the $R(H_{dec})$ dependence (see Fig. 5) and, at $\alpha_{PM} = 3$ and 5, the minimum field in the $B_{eff}(H_{dec})$ dependence significantly exceeds the region $R(H_{dec}) = 0$ observed in the experiment. Therefore, if the PM subsystem affects the field in the intergrain medium, then this effect is insignificant. We can state that the agreement between the behavior of the experimental $R(H)$ dependence and the $B_{eff}(H)$ dependence is only observed when the parameter α_{PM} is about unity. This indicates the absence of compression of the magnetic induction lines from the PM moments in the intergrain medium.

4. CONCLUSIONS

In the granular HTS $HoBa_2Cu_3O_{7-\delta}$, the magnetic moments of holmium atoms behave as an independent paramagnetic subsystem. An analysis of the magnetoresistance hysteresis basing on the concept of an effective field in the intergrain medium (Eq. (2)) showed that the paramagnetic subsystem almost does not affect the effective field in the intergrain medium. This indicates a fundamental difference of the redistribution of the magnetic induction lines in a granular HTS from the superconducting response (the Meissner currents and Abrikosov vortices) and the paramagnetic moments of holmium atoms. In the intergrain medium, the magnetic induction lines from the Meissner currents and Abrikosov vortices are concentrated. Due to the flux compression, the field in the intergrain medium differs significantly from the external field and, under certain conditions (with an increase in the external field), can exceed it by an order of magnitude. The magnetic induction lines from the paramagnetic moments are not concentrated in the intergrain medium, but close, passing through HTS grains. The effect of the paramagnetic moments on the effective field in the intergrain medium is negligible. The quantitative analysis of the paramagnetic contribution to the total magnetization of the $HoBa_2Cu_3O_{7-\delta}$ HTS sample showed that this contribution is made by the holmium magnetic moments located in the cores of the Abrikosov vortices and in the surface region of grains with a thickness comparable with the magnetic field penetration depth. Consequently, the magnetic induction lines from the magnetic ions are closed when passing through these regions.

We dedicate this study to the memory of Vitaly Aleksandrovich Finkel (Kharkiv Institute of Physics and Technology), who passed away in March, 2021. His works, both cited here and others, are important for understanding the mechanisms of magnetoresistance of granular superconductors.

ACKNOWLEDGMENTS

The authors are grateful to V.M. Sosnin, K.A. Shaikhutdinov, and A.A. Krasikov for discussion of the results and I.V. Nemtsev for the electron microscopy investigations of the sample.

The microstructure investigations and a part of the magnetic measurements were carried out on the equipment of the Krasnoyarsk Territorial Center for Collective Use, Krasnoyarsk Scientific Center, Siberian Branch, Russian Academy of Sciences.

FUNDING

This study was supported by the Russian Foundation for Basic Research, the Government of the Krasnoyarsk krai, and the Krasnoyarsk Territorial Foundation for Support of Scientific and R&D Activities, project no. 20-42-240008 "Effect of introduction of paramagnetic ions of rare-earth elements on the superconducting properties of YBCO materials."

CONFLICT OF INTEREST

The authors declare that they have no conflicts of interest.

REFERENCES

1. M. A. Dubson, S. T. Herbet, J. J. Calabrese, D. C. Harris, B. R. Patton, and J. C. Garland, Phys. Rev. Lett. **60**, 1061 (1988).

2. L. Ji, M. S. Rzchowski, N. Anand, and M. Tinkham, Phys. Rev. B **47**, 470 (1993).
3. M. Prester, Supercond. Sci. Technol. **11**, 333 (1998).
4. A. C. Wright, K. Zhang, and A. Erbil, Phys. Rev. B **44**, 863 (1991).
5. C. Gaffney, H. Petersen, and R. Bednar, Phys. Rev. B **48**, 3388 (1993).
6. H. S. Gamchi, G. J. Russell, and K. N. R. Taylor, Phys. Rev. B **50**, 12950 (1994).
7. R. J. Soulen, T. L. Francavilla, W. W. Fuller-Mora, M. M. Miller, C. H. Joshi, W. L. Carter, A. J. Rodenbush, M. D. Manlief, and D. Aized, Phys. Rev. B **50**, 478 (1994).
8. D. H. Liebenberg, R. J. Soulen, T. L. Francavilla, W. W. Fuller-Mora, P. C. McIntyre, and M. J. Cima, Phys. Rev. B **51**, 11838 (1995).
9. R. J. Soulen, T. L. Francavilla, A. R. Drews, L. Toth, M. S. Osofsly, W. L. Lechter, and E. F. Skelton, Phys. Rev. B **51**, 1393 (1995).
10. W. M. Tieran, R. Joshi, and R. B. Hallock, Phys. Rev. B **48**, 3423 (1993).
11. Y. Zhao, X. B. Zuge, J. M. Xu, and L. Cao, Phys. Rev. B **49**, 6985 (1994).
12. L. Urba, C. Acha, and V. Bekeris, Phys. C (Amsterdam, Neth.) **279**, 95 (1997).
13. E. Hannachi, M. K. Ben Salem, Y. Slimani, A. Hamrita, M. Zouaoui, F. Ben Azzouz, and M. Ben Salem, Phys. B (Amsterdam, Neth.) **430**, 52 (2013).
14. E. Hannachi, Y. Slimani, A. Ekicibil, A. Manikandan, and F. Ben Azzouz, J. Mater. Sci.: Mater. Electron. **30**, 8805 (2019).
15. Y. Slimani, E. Hannachi, A. Hamrita, M. K. Ben Salem, M. Zouaoui, M. Ben Salem, and F. Ben Azzouz, J. Supercond. Nov. Magn. **28**, 487 (2015).
16. S. Shifang, Z. Yong, P. Guoqian, Y. Daoq, Z. An, C. Zuyao, Q. Yitai, K. Eiyan, and Z. Qirui, Europhys. Lett. **6**, 359 (1988).
17. Y. J. Quian, Z. M. Tang, K. Y. Chen, B. Zhou, J. W. Qui, B. C. Miao, and Y. M. Cai, Phys. Rev. B **39**, 4701 (1989).
18. P. Múne, F. C. Fonseca, R. Muccillo, and R. F. Jardim, Phys. C (Amsterdam, Neth.) **390**, 363 (2003).
19. C. A. M. dos Santos, M. S. da Luz, B. Ferreira, and A. J. S. Machado, Phys. C (Amsterdam, Neth.) **391**, 345 (2003).
20. N. D. Kuz'michev, JETP Lett. **74**, 262 (2001).
21. N. D. Kuz'michev, Phys. Solid State **43**, 2012 (2001).
22. T. V. Sukhareva and V. A. Finkel, J. Exp. Theor. Phys. **107**, 787 (2008).
23. T. V. Sukhareva and V. A. Finkel', Phys. Solid State **50**, 1001 (2008).
24. V. V. Derevyanko, T. V. Sukhareva, and V. A. Finkel, Tech. Phys. **53**, 321 (2008).
25. T. V. Sukhareva and V. A. Finkel', Phys. Solid State **52**, 452 (2010).
26. M. E. McHenry, P. P. Maley, and J. O. Willis, Phys. Rev. B **40**, 2666 (1989).
27. E. Altshuler, J. Musa, J. Barroso, A. R. R. Papa, and V. Venegas, Cryogenics **33**, 308 (1993).
28. J. López, P. Múne, S. Garsía, and E. Altshuler, Phys. C (Amsterdam, Neth.) **272**, 13 (1996).
29. D. A. Balaev, D. M. Gokhfel'd, A. A. Dubrovskii, S. I. Popkov, K. A. Shaikhutdinov, and M. I. Petrov, J. Exp. Theor. Phys. **105**, 1174 (2007).
30. A. V. Mitin, Phys. C (Amsterdam, Neth.) **235–240**, 3311 (1994).
31. D. López and F. de la Cruz, Phys. Rev. B **43**, 11478 (1991).
32. D. López, . Decca, and RF. de la Cruz, Supercond. Sci. Technol. **5**, S276 (1992).
33. J. L. Giordano, J. Luzuriaga, A. Badía-Majós, G. Nieva, and I. Ruíz-Tagle, Supercond. Sci. Technol. **19**, 385 (2006).
34. D. A. Balaev, A. A. Bykov, S. V. Semenov, S. I. Popkov, A. A. Dubrovskii, K. A. Shaikhutdinov, and M. I. Petrov, Phys. Solid State **53**, 922 (2011).
35. S. V. Semenov, D. A. Balaev, M. A. Pochekutov, and D. A. Velikanov, Phys. Solid State **59**, 1291 (2017).
36. E. B. Sonin, JETP Lett. **47**, 496 (1988).
37. M. Mahel' and J. Pivarč, Phys. C (Amsterdam, Neth.) **308**, 147 (1998).
38. O. V. Gerashchenko and S. L. Ginzburg, Supercond. Sci. Technol. **13**, 332 (2000).
39. M. S. da Luz, C. A. M. dos Santos, B. Ferreira, and A. J. S. Machado, Phys. C (Amsterdam, Neth.) **408–410**, 460 (2004).
40. A. Sukhanov and V. Omel'chenko, J. Low Temp. Phys. **30**, 452 (2004).
41. D. Daghero, P. Mazzetti, A. Stepanescu, and P. Tura, Phys. Rev. B **66**, 11478 (2002).
42. D. A. Balaev, S. I. Popkov, E. I. Sabitova, S. V. Semenov, K. A. Shaykhutdinov, A. V. Shabanov, and M. I. Petrov, J. Appl. Phys. **110**, 093918 (2011).
43. D. A. Balaev, S. V. Semenov, and M. I. Petrov, J. Supercond. Nov. Magn. **27**, 1425 (2014).
44. D. A. Balaev, S. I. Popkov, K. A. Shaikhutdinov, M. I. Petrov, and D. M. Gokhfeld, Phys. Solid State **56**, 1542 (2014).
45. D. A. Balaev, S. V. Semenov, and M. A. Pochekutov, J. Appl. Phys. **122**, 123902 (2017).
46. S. V. Semenov and D. A. Balaev, Phys. C (Amsterdam, Neth.) **550**, 19 (2018).
47. S. V. Semenov and D. A. Balaev, J. Supercond. Nov. Magn. **32**, 2409 (2019).
48. S. V. Semenov, D. A. Balaev, and G. Ya. Ataeva, Phys. Solid State **62**, 1136 (2020).
49. D. A. Balaev, S. V. Semenov, and D. M. Gokhfeld, J. Supercond. Nov. Magn. **34**, 1067 (2021).
50. S. V. Semenov, D. A. Balaev, and M. I. Petrov, Phys. Solid State **63** (7), 986 (2021).
51. S. V. Semenov, A. D. Balaev, and D. A. Balaev, J. Appl. Phys. **125**, 033903 (2019).
52. H. Theuss and H. Kronmüller, Phys. C (Amsterdam, Neth.) **242**, 155 (1995).
53. M. R. Koblischka and M. Murakami, J. Supercond.: Incorpor. Nov. Magn. **14**, 415 (2001).
54. E. Altin, D. M. Gokhfeld, F. Kurt, and Z. D. Yakinci, J. Mater. Sci.: Mater. Electron. **24**, 5075 (2013).

55. A. Öztürk, M. Dogăn, Í. Düzgün, and S. Celebi, J. Supercond. Nov. Magn. **29**, 1787 (2016).
56. D. M. Gokhfeld, D. A. Balaev, I. S. Yakimov, M. I. Petrov, and S. V. Semenov, Ceram. Int. **43**, 9985 (2017).
57. B. W. Lee, J. M. Ferreira, Y. Dalichaouch, M. S. Torikachvili, K. N. Yang, and M. B. Maple, Phys. Rev. B **37**, 2368 (1988).
58. A. D. Balaev, Yu. V. Boyarshinov, M. M. Karpenko, and B. P. Khrustalev, Prib. Tekh. Eksp., No. 3, 167 (1985).
59. D. A. Balaev, A. G. Prus, K. A. Shaykhutdinov, D. M. Gokhfeld, and M. I. Petrov, Supercond. Sci. Technol. **20**, 495 (2007).
60. V. V. Derevyanko, T. V. Sukhareva, and V. A. Finkel, Phys. Solid State **60**, 470 (2018).
61. T. V. Sukhareva and V. A. Finkel, JETP Lett. **108**, 243 (2018).
62. T. V. Sukhareva and V. A. Finkel, J. Low Temp. Phys. **44**, 194 (2018).
63. T. V. Sukhareva and V. A. Finkel, J. Low Temp. Phys. **46**, 550 (2020).
64. K. Osuch, Phys. C (Amsterdam, Neth.) **383**, 263 (2002).
65. C. P. Bean, Rev. Mod. Phys. **36**, 31 (1964).
66. D. M. Gokhfeld, Tech. Phys. Lett. **45**, 1 (2019).
67. D. N. Zheng, A. M. Campbell, J. D. Johnson, J. R. Cooper, F. J. Blunt, A. Porch, and P. A. Freeman, Phys. Rev. B **49**, 1417 (1994).
68. G. Blatter, M. V. Feigel'man, V. B. Gekshkebein, A. I. Larkin, and V. M. Vinokur, Rev. Mod. Phys. **66**, 1125 (1994).
69. D. A. Balaev, A. A. Dubrovskii, K. A. Shaikhutdinov, S. I. Popkov, D. M. Gokhfeld, Yu. S. Gokhfeld, and M. I. Petrov, J. Exp. Theor. Phys. **108**, 241 (2009).
70. D. A. Balaev, A. A. Dubrovskii, S. I. Popkov, D. M. Gokhfeld, S. V. Semenov, K. A. Shaikhutdinov, and M. I. Petrov, Phys. Solid State **54**, 2155 (2012).
71. D. A. Balaev, S. V. Semenov, and M. I. Petrov, Phys. Solid State **55**, 2422 (2013).
72. A. Altinkok, K. Kilic, M. Olutas, and A. Kilic, J. Supercond. Nov. Magn. **26**, 3085 (2013).

Translated by E. Bondareva